Auxetic nuclei in embryonic stem cells exiting pluripotency

Stefano Pagliara[1†], Kristian Franze[2†], Crystal R. McClain[1,3], George W. Wylde[1], Cynthia L. Fisher[4], Robin J. M. Franklin[3], Alexandre J. Kabla[5], Ulrich F. Keyser[1] and Kevin J. Chalut[1,4*]

Embryonic stem cells (ESCs) self-renew in a state of naïve pluripotency in which they are competent to generate all somatic cells. It has been hypothesized that, before irreversibly committing, ESCs pass through at least one metastable transition state. This transition would represent a gateway for differentiation and reprogramming of somatic cells. Here, we show that during the transition, the nuclei of ESCs are auxetic: they exhibit a cross-sectional expansion when stretched and a cross-sectional contraction when compressed, and their stiffness increases under compression. We also show that the auxetic phenotype of transition ESC nuclei is driven at least in part by global chromatin decondensation. Through the regulation of molecular turnover in the differentiating nucleus by external forces, auxeticity could be a key element in mechanotransduction. Our findings highlight the importance of nuclear structure in the regulation of differentiation and reprogramming.

Understanding the trajectory between naïve pluripotency and lineage restriction is crucial for ESC research[1–3], much of it focusing on defining a transcriptional and epigenetic ESC 'state space'[4–6]. It is widely believed that there must be a fulcrum of 'precarious balance'[7]—a hypothetical transitional pluripotent state which is metastable in nature—from which ESCs have a choice to return to a naïve pluripotent state or irreversibly prime for differentiation. If a clear definition of the transition could be established, this could be used as a gateway to control differentiation and reprogramming[8,9].

To construct a definition of a naïve pluripotency (N), transition (T), and differentiation priming (P) in mouse ESCs, we used a *Rex1*GFPd2 reporter[10] (Fig. 1a and Supplementary Fig. 1). *Rex1* is a specific marker for pluripotency, and its downregulation accompanies irreversible exit from pluripotency in ESCs (ref. 11). Naïve pluripotency is maintained by 2i+LIF medium, which is N2B27 medium supplemented with MEK inhibitor, GSK3 inhibitor and Leukemia inhibitory factor (LIF; see Methods and ref. 12). Removing the inhibitors initiates ESC differentiation. We defined ESCs to be in transition (T-ESCs) when they reached a time point after which *Rex1*GFPd2 expression is prone to change. Using a culturing procedure (Methods) we identified this time point to be 24 h (Supplementary Fig. 1). Although they have not downregulated *Rex1*GFPd2, T-ESCs at this time point have downregulated the pluripotency factor *Nanog* (Supplementary Fig. 2), but can be returned to N-ESCs in 2i+LIF medium for an indefinitely self-renewing ESC culture (data not shown, personal communication with Austin Smith). ESCs cultured in N2B27 after 24 h and before 48 h are expressing *Rex1*GFPd2 heterogeneously (Supplementary Fig. 1). P-cells, which we obtained after 48 h in N2B27 medium, have entirely downregulated *Rex1*GFPd2 and cannot generally be reverted to N-ESCs without reprogramming; P-cells are nonetheless distinct from lineage restricted cells. With these defined N-ESCs, T-ESCs, and P-cells, we explored the mechanical properties of differentiating ESCs.

Transition ESCs have an auxetic nucleus

We used atomic force microscopy (AFM, CellHesion 200, JPK Instruments AG) to measure the apparent reduced modulus $K = E/(1 - \nu^2)$ of the cells[13,14] (Fig. 1b and Supplementary Methods). K is related to two standard material properties, Young's modulus E, which is a measure of elastic uniaxial stiffness (the larger E the stiffer the material), and the Poisson's ratio ν, which relates the change in length of a material that is subject to a force to the accompanying change in its cross-section. Poisson's ratio is the negative ratio of transverse and longitudinal normalized deformation. Almost all common materials become thinner when stretched and therefore have a positive Poisson's ratio.

At low indentation depths ($\delta \leq 1\,\mu m$), K was similar in all cell groups (average values of $130\,Pa < K < 180\,Pa$). Whereas K of N-ESCs and P-cells did not change at larger indentations (δ up to $3\,\mu m$), surprisingly K of T-ESCs significantly increased with increasing compression (Fig. 1c; $P_N = 0.69$, $P_P = 0.71$, $P_T = 5.5 \times 10^{-16}$, 1-way ANOVA). As the cell sizes of N- and T-ESCs were nearly identical (Supplementary Fig. 3), this stiffening was not attributable to a substrate effect that would emerge as a consequence of a decreased cell height[15].

Because in all investigated cell populations the nucleus takes up a large part of the cell volume, and because nuclei contribute significantly to cell stiffness[14], we investigated how nuclear deformation is involved in the cellular response to the applied stress. Cells were labelled with Syto13 (Invitrogen), a nucleic acid dye suitable for live cells, and imaged during AFM measurements using epifluorescence microscopy (Fig. 1b). The signal intensity of Syto13 is three to four times higher in the nucleus than in the
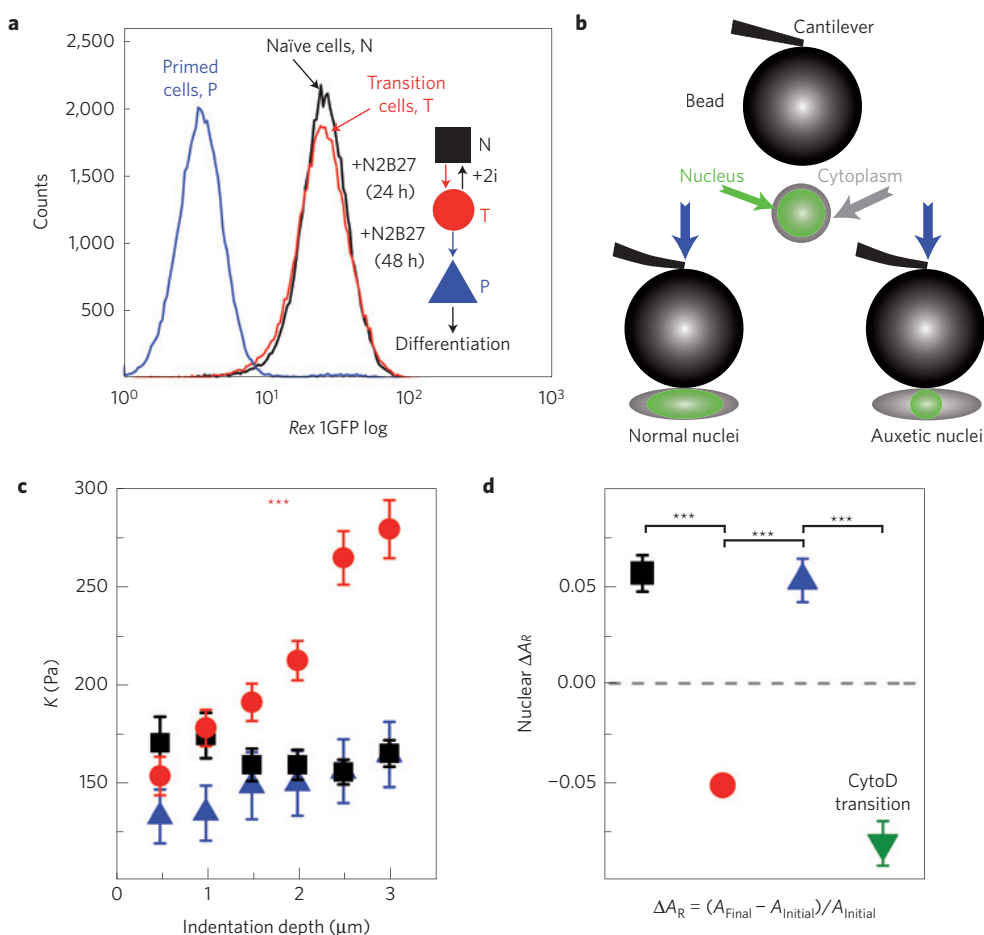
Figure 1 | Atomic force microscopy measurements of ESCs. a, *Rex1*GFPd2 profiles of ESCs at different stages during differentiation, and a schematic demonstrating the culturing protocol to define the ESC states (inset). **b**, Cartoon depicting the applied compressive load and the cell response for different cell types (not to scale, bead is ~37 µm while average cell size is ~13 µm). Both cytoplasm and nuclear deformation are measured by cross-sectional area. **c**, K measured at different indentation depths δ for N-ESCs, T-ESCs and P-cells. Whereas K of N-ESCs and P-cells remains constant, K of T-ESCs significantly increases with indentation depth. The numbers of independent experiments and measured cells, (M, m), are (3,56), (3,56) and (1,21), respectively. **d**, Relative change in the nuclear cross-sectional area on compressing N-ESCs, T-ESCs, P-cells and CytoD-treated T-ESCs by 2 µm. (M, m) are (3,98), (3,117), (3,53) and (2,32), respectively. The dashed line denotes a cross-sectional area change of zero. Materials below this line, including T-ESCs and CytoD-treated T-nuclei, are auxetic. *** indicates $P < 1 \times 10^{-5}$ by a 1-way ANOVA test, and error bars are standard error of the mean, in all the text and figure captions unless otherwise noted.

cytoplasm; we used this contrast for reliable discernment between the two (Supplementary Information and Supplementary Fig. 4). The cytoplasm of all investigated cell types, as well as the nuclei of N-ESCs and P-cells, and lineage restricted extraembryonic (XEN) cells, significantly increased in cross-sectional area by ~5–10% on compression by 2 µm with the AFM probe, as expected (Fig. 1d and Supplementary Fig. 5). Remarkably, however, the nuclei of T-ESCs became smaller by ~5–10% in cross-sectional area on compression (Fig. 1d), which implied that the T nuclei have a negative Poisson's ratio (that is, they are auxetic). The stiffening of T-ESCs with increasing compression described above is also a signature of auxetic materials, because auxetic materials become denser with compression[16]. The nucleus of T-ESCs remained auxetic even after a 10 min treatment with 1 µM of the actin-depolymerizing drug Cytochalasin D (CytoD, Supplementary Information and Fig. 1d). These AFM studies thus strongly imply that the T-nuclei, in contrast to the N- and P-nuclei, are auxetic, and this auxeticity exists independent of the actin cytoskeleton.

To further demonstrate the auxeticity of nuclei of T-ESCs with higher throughput, and under tension as opposed to compression, we developed an optofluidic assay. This assay allowed us

to confine single ESCs in a microchannel (Fig. 2a–d and Supplementary Figs 6 and 7 and Video 1). We recorded fluorescence microscopy videos of cells stained with Syto13 passing through the channels (Supplementary Video 2), and used images of the same cell before entering the channel, during translocation, and after exiting the channel (Fig. 2b–d) for deformation analysis. Ellipses were fitted to the cell and the nucleus, yielding axial and transverse strain, S_A and S_T, respectively (Fig. 2e). These quantities were used to measure changes in cell and nuclear morphology of N- and T-ESCs, P-cells, XEN, HL60 and HeLa cells (Supplementary Information) as well. In this assay, nuclear deformation is largely driven by two components. First, nuclei larger than the channel width directly experience a transverse compression, an effect that should become increasingly insignificant for nuclei smaller than the channel width. In addition, all nuclei experience stretching stresses caused by cytoskeletal strain when the cell is confined in the channel.

Despite their similar size (Supplementary Fig. 3), T-ESCs translocated the channels faster than N-ESCs and P-cells (Supplementary Fig. 8), suggesting a higher overall deformability in T-ESCs when stretched. We found no significant differences in overall cell
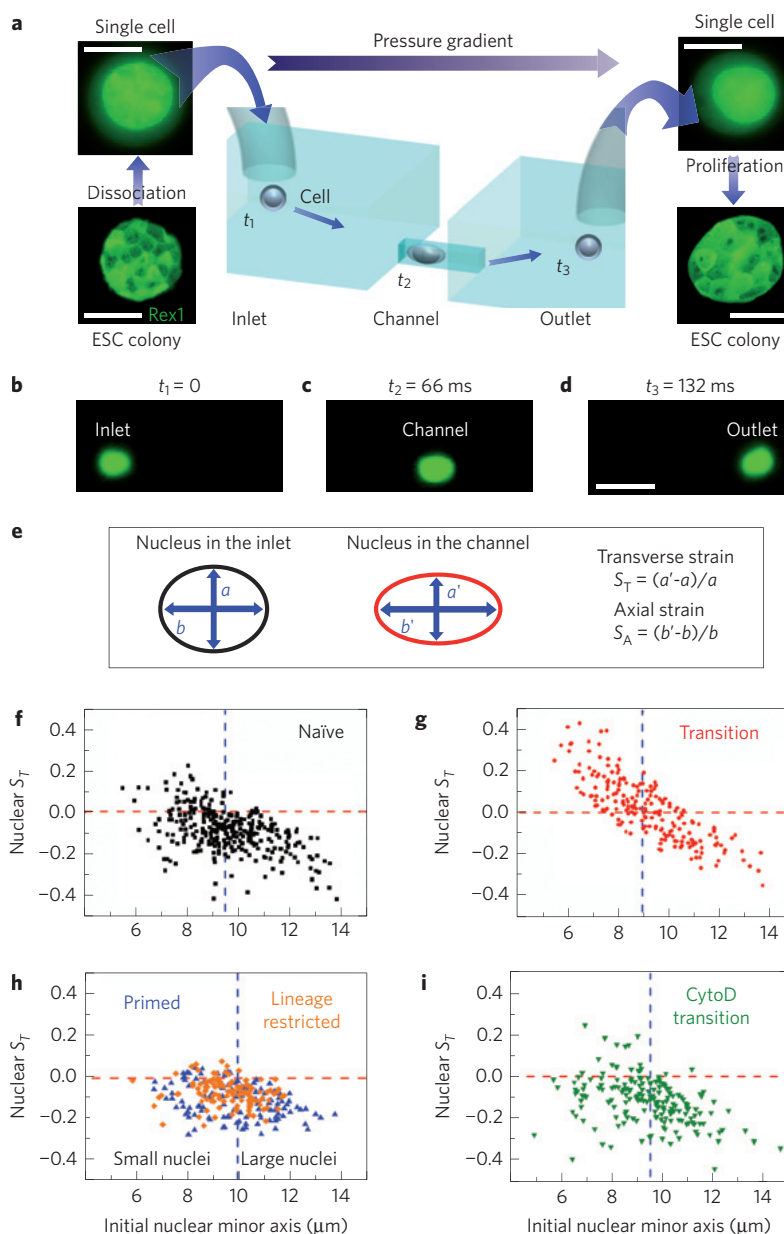
639

Figure 2 | Optofluidic assay. a, ESCs are detached from the culture plate, resuspended as single cells and loaded in the inlet of the microfluidic chip. The applied pressure gradient powers the transport of single cells from the inlet to the outlet. The inlet and outlet reservoirs are connected via channels smaller than the average cell size; therefore, cells must squeeze through the channels. Single cells collected from the outlet form colonies of fully functioning ESCs. Scale bars, 10 and 50 μm for single cells and colonies, respectively. **b–d**, Three consecutive epi-fluorescence snapshots of a Syto13-labelled cell translocating the channel from the inlet to the outlet under an applied pressure of 10 mbar. The detected fluorescence signal allows the simultaneous measurement of both cell and nuclear deformation. Scale bar, 25 μm. **e**, Schematic of nuclear shape whilst the cell is the inlet (left) and in the channel (right). We quantify nuclear deformation by using the transverse, S_T, and axial strains, S_A, where a (b) and a' (b') are the nuclear transverse (axial) extents in the inlet and in the channel, respectively. **f–i**, Scatter plots correlating the transverse nuclear strain S_T in the channel to the initial nuclear minor axis for N-ESCs (squares), T-ESCs (circles), P-cells (upward triangles), lineage restricted HL60 cells (diamonds) and T-ESCs treated with Cytochalasin D (downward triangles). $M = 3, 3, 2, 1$ and 2, respectively. A negative (positive) strain denotes a decrease (increase) of the nuclear transverse extent while the cell squeezes through the channel. The horizontal lines denotes a nuclear S_T of zero and the vertical line is the population median for each data set used to separate the population of each class of cells in small and large nuclei categories. Small T-ESC nuclei show a markedly different behaviour from all other investigated cell types: their S_T increases above 0, indicative of auxeticity.

deformation in the channels across cell types, although there was an overall loss of volume (as extrapolated from cross-section, assuming spheroidal cells) in all cells (Supplementary Fig. 9), which was observed in previous reports[17]. Nuclear deformation in the channel, however, strongly depended on the ESC stage. The axial elongation S_A was largest for T-ESCs compared with other cell types

(Supplementary Fig. 10). Moreover, when their nucleus was smaller than the channel width, and compressive stresses from the channel thus became less significant, S_T in T-nuclei—in contrast to N- and P-nuclei—was positive (Fig. 2g and Supplementary Fig. 10).

Our nuclear strain analysis (Fig. 2f–i) is further evidence of the auxeticity of the T-nucleus for the following reasons. Nuclear
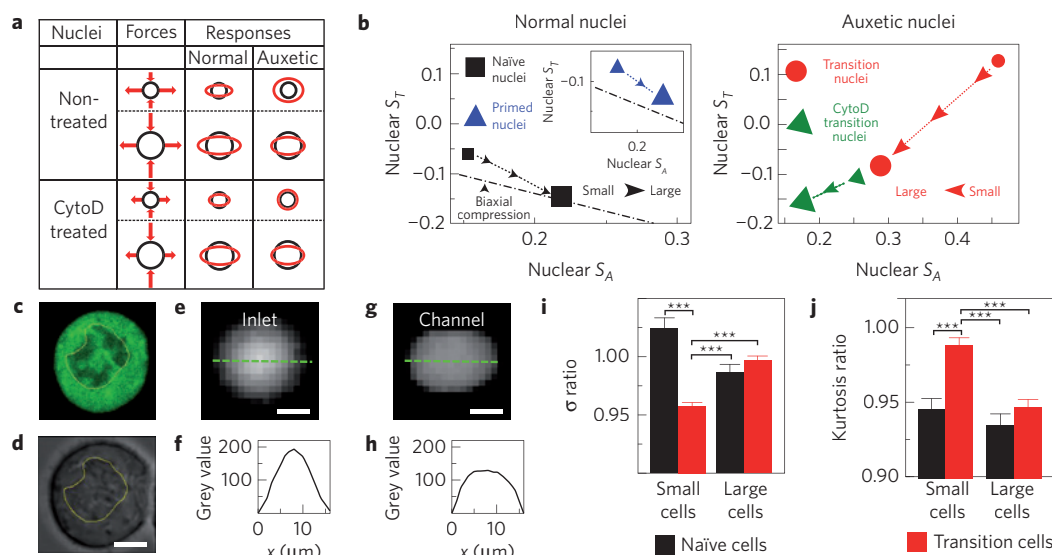
Figure 3 | Normal and auxetic nuclei. a, Depiction of stresses (arrows in the second column) acting on small and large nuclei as defined in Fig. 2f–i (small and large black circles, respectively) for cells untreated and treated with Cytochalasin D. Size of arrows indicates relative force. The normal and auxetic nucleus response is depicted in the third and fourth column, respectively, where the red shapes representing the deformed nuclei are overlapped with the original nuclear shape (black circle). **b**, Correlation between transverse and axial nuclear strain for normal and auxetic nuclei. The dotted arrows are guides for the eye denoting the trend from small to large nuclei (small and large symbols, respectively). Designation of small and large nuclei is determined from the cut-off shown in Fig. 2f–i. N-nuclei (squares) and P-nuclei (inset, upward triangles) present a 'normal' response: on increasing the nuclear size (from small to large symbol) the nuclear S_T becomes more negative whereas the nuclear S_A increases. This is qualitatively in agreement with simple biaxial compression models (dashed dotted line; for information about models see Supplementary Information). T-nuclei (circles) clearly exhibit an auxetic behaviour: on increasing the nuclear size the nuclear S_T changes sign from positive for small nuclei to negative for large nuclei, whereas the ratio of S_A for small to large nuclei is nearly 2. S_A presents the same trend in T nuclei treated with Cytochalasin D (green triangles). Error bars are reported in Supplementary Fig. 10. **c,d**, Bright-field and epifluorescence images, respectively, of a T-ESC after fluorescein incubation, imaged through a 60× objective (NA = 1.4). Scale bar, 5 μm. **e–h**, Epifluorescence images and corresponding grey value profiles (imaged through a 40× objective with NA = 0.6, and measured along the dashed line) of a T-ESC loaded with fluorescein before (**e,f**) and on entering the microfluidic channel (**g,h**), respectively. The apparent signal is higher in the centre of the cell, where this is thicker. Scale bars, 5 μm. **i,j**, Ratio between the profile standard deviations σ (**i**) and kurtosis k (**j**) (inside/outside channel) for naïve (black) and transition (red) cells (Supplementary Fig. 15). (M, m) are (3,270) and (3,317), respectively. The decrease in σ and increase in k for small T-ESCs suggest that fluorophores are driven towards the centre of the stretched cells; that is, the nuclear signal increases at the expense of the signal from the cytoplasm.

deformation depends partly on the channel geometry, with a shift between positive and negative S_T occurring in T-ESCs at an initial nuclear minor axis of ~9 μm. Given the channel size of 11 μm and that cytoplasm is surrounding the nucleus, this shift is probably due to the fact that larger nuclei start to experience more direct compression by the imposed geometric constraints. To further investigate this phenomenon, we distinguished between small and large nuclei by the median of the nuclear size data (dashed blue line in Fig. 2f–i, using the short axis of the ellipse as the size). We predicted the following two possible strain responses based on considerations of elastic materials (Fig. 3a). First, in non-auxetic materials, all nuclei should have a negative S_T. Additionally, smaller nuclei will experience an axial stretch but a smaller transverse compression than the larger nuclei; therefore, the larger nuclei should possess a larger S_A than the smaller nuclei. Second, in auxetic materials, as the effects of compression and stretch would tend to counteract each other, the larger nuclei should possess a smaller S_A than the smaller nuclei. Furthermore, S_T should be positive for smaller nuclei and negative for larger nuclei.

The first prediction was true for the N- and P-nuclei, as well as for the HL60, XEN, and HeLa nuclei (Supplementary Figs 10 and 11). In contrast, the second prediction was true for T-nuclei: the larger T-nuclei experienced less S_A than the smaller T-nuclei, and the smaller T-nuclei had a positive S_T (Supplementary Fig. 10).

To test whether the expansion during stretching in the T-nuclei was caused by tensile forces arising from the actin cytoskeleton,

we used the CytoD treatment described above on T-ESCs (Supplementary Information). S_A in the nuclei diminished by over 50%, and the positive S_T observed in the smaller nuclei of the untreated T-ESCs largely disappeared (Fig. 2i and Supplementary Fig. 10). This confirms that the transverse expansion seen in untreated T-nuclei is caused by the cytoskeletal stretch. The fact that CytoD-treated small T-nuclei exhibited negative transverse strain can be explained by a change in the balance between compression from the channel walls and reduced tension transmitted through the perturbed actin cytoskeleton; the induced cross-sectional contraction of the compressed auxetic nucleus here overwhelms the (reduced) stretch transmitted through the cytoskeleton. These nuclei are thus still auxetic and, accordingly, after treatment the larger nuclei experienced smaller S_A than the smaller nuclei (Supplementary Fig. 10).

We summarized the results in Fig. 3. After separating the large and small nuclei of each cell group by median size (as in Fig. 2f–i), we plot S_T versus S_A. For materials with a positive Poisson's ratio experiencing a biaxial compression or uniaxial stretch, there would be a negative slope going from small to large nuclei (Supplementary Information). This negative slope was observed in N-ESCs, P-, HL60, XEN, and HeLa cells, and their corresponding nuclei; however, the exact opposite trend was observed for T-nuclei (CytoD-treated and untreated, Fig. 3b and Supplementary Fig. 11), but not the cells themselves (data not shown), a further indication of the T-nuclei's auxetic behaviour. Therefore, we defined the auxetic

phenotype seen in T-nuclei as shown in Fig. 3b: at a population level, the nuclear S_T and S_A are larger in smaller nuclei than they are in larger nuclei.

Auxeticity facilitates molecular turnover in the nucleus

Auxeticity has profound volume implications: stretched auxetic materials will experience a significant volume expansion. We first verified the volume changes that would be intrinsic to an auxetic nucleus with confocal microscopy of Syto 13-labelled cells (Supplementary Fig. 12) and a Hoechst-based assay (Supplementary Fig. 13). Furthermore, the pronounced nuclear-volume changes arising from stretch of the nucleus would imply a concomitant flow of fluid and small molecules into the nucleus. To show this, we loaded both N- and T-ESCs with fluorescein. In relaxed cells, the dye was significantly more concentrated in the cytoplasm, indicating that there is more available space in the cytoplasm than in the nucleus through which the molecules can freely diffuse (Fig. 3c,d). In auxetic materials, the volume and with it the porosity[18] (or void fraction, that is, the available space) should increase on stretch (Supplementary Fig. 14), and the otherwise more densely packed nucleus should provide a largely enhanced space into which small molecules can diffuse. Indeed, we found a strong increase in the nuclear signal at the expense of signal from the cytoplasm in the T-ESCs, but not in the N-ESCs. To quantify this, we extracted a profile of the fluorescence intensity both before the cell entered the channel and inside the channel (Fig. 3e–h). We then inferred three quantities from each intensity profile: the axial length of the cell s, the standard deviation σ of the profile, and its kurtosis k, defined as the fourth moment of the distribution normalized by σ (ref. 4). Qualitatively, kurtosis characterizes the flatness of a distribution: the lower the kurtosis, the flatter and less peaked the distribution, and in the case of these experiments the more equally distributed the dye. If fluorophores move into the nucleus and thus towards the centre of a cell, we expect that σ will decrease, and that k will increase, as explained in Supplementary Fig. 15. Accordingly, σ increased in the channel in small N-ESCs but decreased in small T-ESCs, whereas k showed the opposite trend (Fig. 3i,j), which strongly suggests that fluorophores are driven towards the centre of small T-ESCs when stretched, but not in small N-ESCs. This also suggests that fluorophores enter the cell nucleus while its volume increases on deformation, indicating a possible function for auxeticity: external stresses in the developing embryo could thus drive an increase in molecular turnover in the nucleus of T-ESCs during differentiation.

Chromatin decondensation drives auxetic phenotype

To address possible mechanisms for the auxeticity we investigated chromatin condensation states, and, given recent reports about their importance for mechanosensing[19], nuclear lamins. Lamin A/C expression was low to undetectable, and we did not observe any consistent change in the expression of *Lmna* or *Lmnb1* by qRT-PCR (Supplementary Fig. 2) or immunofluorescence (data not shown) across the ESC groups, although the nuclear envelope of the T-nuclei was significantly less wrinkled than the N- and P-nuclei (Fig. 4a–b and Supplementary Fig. 16). Electron microscopy images showed considerable differences in global chromatin-condensation levels between the three states. A quantitative analysis revealed that the chromatin of T-nuclei is significantly less condensed than in the N- and P-nuclei (Fig. 4c). To further investigate the role of chromatin decondensation in nuclear auxecity, we treated N-ESCs with 300 nM of Trichostatin A (TSA), an HDAC inhibitor that globally decondenses chromatin. TSA treatment caused the cells to become auxetic: as in the T-ESCs, the apparent reduced modulus K of TSA-treated N-ESCs significantly increased with increasing indentation δ (Fig. 4d), the nuclear cross-sectional area shrank under compression with AFM (Fig. 4e and Supplementary Fig. 5),
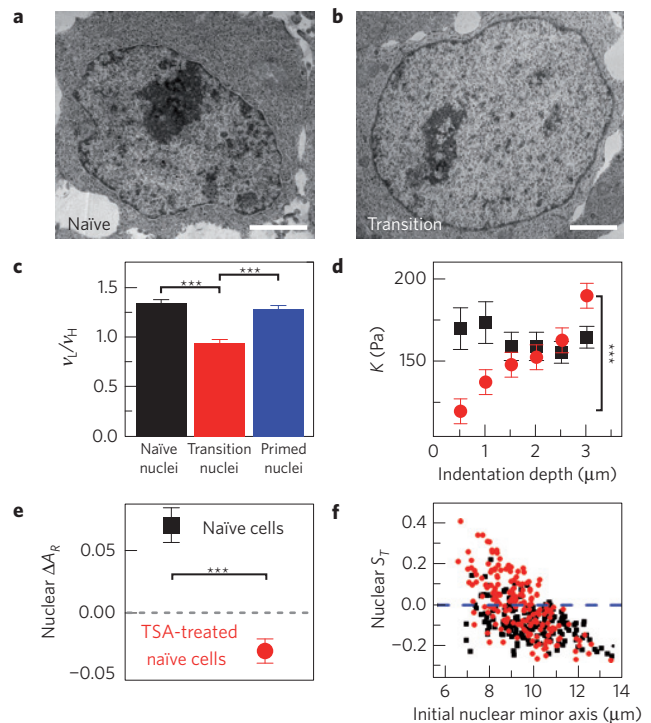
Figure 4 | Auxeticity and chromatin condensation states.
a,b, Representative electron microscopy images of N-ESCs (**a**) and T-ESCs (**b**), suggesting a less densely packed nucleus in T-ESCs. Scale bars, 3 μm. **c**, Corresponding measurements of the ratio between low frequencies ν_L (corresponding to wavelengths $\lambda > 100$ nm) and high frequencies ν_H (corresponding to wavelengths $10 < \lambda < 100$ nm) calculated from the 2D Fourier spectrum (see Supplementary Information). The ratio is significantly lower for T-nuclei compared with N- and P-nuclei, indicating that chromatin is less densely packed (more uniform) in T-nuclei. $m = 23, 23$ and 24, respectively. **d**, K measured at different indentation depths δ for N-ESCs (black squares, reprinted from Fig. 1c) and Trichostatin A (TSA) treated N-ESCs (red circles). (M, m) are (3,56) and (3,64). TSA treatment leads to chromatin decondensation, and to an increase of K with δ, as expected for auxetic materials. **e**, Relative change in the nuclear cross-sectional area on compressing N-ESCs and TSA-treated N-ESCs with AFM. (M, m) are (3,98) and (2,63), respectively. The dashed line denotes a cross-sectional area change of zero. Materials below this line are auxetic. **f**, Scatter plot correlating the transverse nuclear strain S_T in the channel to the initial nuclear minor axis for N-ESCs and TSA-treated N-ESCs. $M = 2$ and 4, respectively. Overall, these data imply the involvement of chromatin decondensation in the auxetic phenotype of transition ESC nuclei.

and it increased under stretch in the microfluidic assay (Fig. 4f and Supplementary Fig. 10). Therefore, chromatin-condensation states probably play a significant role in causing the auxetic phenotype.

Possible implications of an auxetic nucleus

The present study provides evidence that transition embryonic stem cells can be distinguished by an auxetic nucleus. Auxetics are rare materials, widely studied in physical and materials sciences[16]; this study presents an extraordinary example of auxeticity in a living material. Auxeticity is a biophysical phenotype, which, like cell and nuclear mechanics, could be important for cell movement in tissue[20] and for modulating the sensitivity of ESCs to physical cues[21–24]. Furthermore, it has been observed that nuclear mechanics and structure are significant for ESCs: nuclei of ESCs stiffen on differentiation[25] and show significant global condensation of chromatin[26]. There is also evidence that the nucleus undergoes dynamic structural and mechanical changes during the

process of differentiation and downstream lineage specification[27,28]. Importantly, the T-ESC exists in a state of heightened chromatin decondensation (indicated from electron microscopy in the current study and ref. 27). Indeed, nuclei of T-ESCs as well as nuclei of N-ESCs with pharmacologically induced decondensed chromatin are auxetic. Furthermore, the strong increase in K under increasing compression found in both T-ESCs and TSA-treated N-ESCs is a signature of an auxetic material.

In addition to establishing a transition phenotype, there are other significant implications of the observed auxeticity. First, auxeticity is a consequence of architecture: it imposes structural rules on the comprising substructures of a material[29]. The findings presented in this paper can guide investigations of the superstructure of the nucleus and of interactions between its comprising substructures. Second, auxeticity in the nucleus—given that it leads to stiffening of materials under compression (Fig. 1c)—could play a crucial role in tissue organization, particularly because transition cells have been observed in the early embryo[30]. Cells of the early embryo have large nuclear to cytoplasmic ratios[31]; therefore, auxeticity could lead to active alteration of the mechanical properties of these cells under stress, thereby affecting their ability to reorganize in tissue. This could dramatically impact the physically driven formation of the pluripotent epiblast[32].

Ultimately, nuclear auxeticity could be crucially involved in the conversion of mechanical stimuli into a cellular response, that is, in mechanotransduction. External stresses could change the volume of T-nuclei, and thus the space available in the nucleus for small molecules such as signalling molecules and transcription factors. T-nuclei exposed to tension, for example, would increase in volume, which could lead to more space for molecules that trigger differentiation; at the same time, cells of the same population but in other parts of the tissue could be compressed, leaving less space for molecules, and thus assume a different fate. Alternatively, the physical properties of T-nuclei in a dynamically remodelling tissue could enhance differentiative capacity by acting as stress-driven auxetic pumps to increase molecular turnover.

Methods

Cell culture. The *Rex1*GFPd2 ESCs used in the current study[10] were used between passage 15 and passage 25, and were cultured on 0.1% gelatin at all times in 2i medium, described in (ref. 12), which is N2B27 medium (Invitrogen) supplemented with MEK inhibitor (1 μM PD0325901) and GSK3 inhibitor (3 μM CHIR99021) plus Leukemia inhibitory factor (LIF). For priming/differentiation protocol, ESCs were passaged and seeded directly into N2B27 medium at a concentration of 4×10^5 cells ml^{-1}. The GFP signal was regularly analysed by flow cytometry using a CyAn ADP analyser (Beckman Coulter, Brea) to monitor *Rex1*GFPd2 expression in the cells, and we titrated the time point of 24 h after seeding in N2B27 to be T-ESCs, and 48 h after seeding in N2B27 to be P-ESCs (Fig. 1a and Supplementary Fig. 1).

Cell preparation. For microfluidics experiments, cells were incubated at 37 °C with 1 μM Syto13 (Invitrogen) for 20 min, and were detached from tissue plastic with Accutase (for ESCs) and Trypsin for XEN and HeLa cells (HL60s are a suspended cell line), and then centrifuged and resuspended in PBS. The cells were then filtered with 20 μm filters (Partec, Munster) to remove aggregates.

For imaging experiments, cells were allowed to settle on glass dishes while they were incubated with 1 μM Syto13 for 20 min. For AFM experiments, cells were passaged three hours before experiments to ensure the ability to measure single cells, and were incubated with 1 μM Syto13 for 20 min before measurement. For all experiments, the time between the cells being taken out of incubation and measured was less than 20 min.

Atomic force microscopy. Monodisperse polystyrene beads (diameter 37.28 ± 0.34 μm, microParticles) were glued to tipless silicon cantilevers (Arrow-TL1, spring constant ∼0.02 Nm^{-1}; NanoWorld, Neuchatel, Switzerland). Cantilevers were mounted on a JPK CellHesion 200 AFM (JPK Instruments AG), which was set up on an inverted optical microscope (Zeiss Axio Observer A1). Cantilever spring constants were determined via the thermal noise method included in the AFM software. See Supplementary Information for further details.

Microfluidic assay. The microfabrication of the fluidic chip relies on multilevel photolithography and replica moulding. For the fabrication of the mould, a layer of SU-8 2005 (Microchem) was deposited via spin coating (1,000 r.p.m. for 30 s) on a silicon wafer and exposed to ultraviolet light (1 s, 365–405 nm, 52 mW cm^{-2}) through a quartz mask (Photodata Ltd) patterned with an array of wires with two different widths, 10 μm and 12 μm. After development, a layer of SU-8 2015 (Microchem) was deposited by spin coating (2000 r.p.m. for 30 s). A second mask patterned with two symmetrical reservoir chambers separated by a 50 μm gap and ending with two 1 mm-side circular pads was aligned relative to the sample through a MJB4 mask aligner (Karl Suss) in a way that positioned the central region of the wires under the 50 μm-gap on the mask. The sample was exposed for 4 s and developed. The thickness of the obtained wires was 10 μm and the thickness of the reservoir was 20 μm as measured by a Dektak stylus profilometer (Veeco, Plainview). Replica molding of the device is realized by casting on it a 9:1 (base:curing agent) polydimethylsiloxane (PDMS) mixture and *in situ* curing at 60 °C for 60 min in an oven. PDMS is bonded to a glass slide by exposing both surfaces to oxygen plasma treatment (8.5 s exposure to 2.5 W plasma power, Plasma etcher, Diener, Royal Oak) thus improving adhesion quality and hydrophilicity. The device is completed by the integration of PEEK tubing connected to a computerized pressure-based flow control system (MFCS-4C, Fluigent) that allows one to regulate the flow in the microfluidic chip. This multi-layer device allows us to achieve—in a single chip—accurate screening and high throughput. Indeed, thanks to the fact that the reservoirs have dimensions larger than the cell size, by applying a pressure gradient we can deliver cells with a high throughput to the channel region. Here, given that the channel's cross-sectional area is smaller than the typical cell dimension (although larger than the typical nucleus), the cells must squeeze through the channels. The resulting slow translocation time (from hundreds of microseconds to a few seconds) enables single cell measurements.

References

1. Betschinger, J. *et al.* Exit from pluripotency is gated by intracellular redistribution of the bHLH transcription factor Tfe3. *Cell* **153**, 335–347 (2013).
2. Silva, J. & Smith, A. Capturing pluripotency. *Cell* **132**, 532–536 (2008).
3. Smith, A. Pluripotent stem cells: Private obsession and public expectation. *EMBO Mol. Med.* **2**, 113–116 (2010).
4. Nichols, J. & Smith, A. Naive and primed pluripotent states. *Cell Stem Cell* **4**, 487–492 (2009).
5. Young, R. A. Control of the embryonic stem cell state. *Cell* **144**, 940–954 (2011).
6. Marks, H. *et al.* The transcriptional and epigenomic foundations of ground state pluripotency. *Cell* **149**, 590–604 (2012).
7. Loh, K. M. & Lim, B. A precarious balance: Pluripotency factors as lineage specifiers. *Cell Stem Cell* **8**, 363–369 (2011).
8. Fisher, C. L. & Fisher, A. G. Chromatin states in pluripotent, differentiated, and reprogrammed cells. *Curr. Opin. Genet. Dev.* **21**, 140–146 (2011).
9. Hanna, J. *et al.* Human embryonic stem cells with biological and epigenetic characteristics similar to those of mouse ESCs. *Proc. Natl Acad. Sci. USA* **107**, 9222–9227 (2010).
10. Wray, J. *et al.* Inhibition of glycogen synthase kinase-3 alleviates Tcf3 repression of the pluripotency network and increases embryonic stem cell resistance to differentiation. *Nature Cell Biol.* **13**, 838–845 (2011).
11. Toyooka, Y., Shimosato, D., Murakami, K., Takahashi, K. & Niwa, H. Identification and characterization of subpopulations in undifferentiated ES cell culture. *Development* **135**, 909–918 (2008).
12. Ying, Q. L. *et al.* The ground state of embryonic stem cell self-renewal. *Nature* **453**, 519–523 (2008).
13. Franze, K. Atomic force microscopy and its contribution to understanding the development of the nervous system. *Curr. Opin. Genet. Dev.* **21**, 530–537 (2011).
14. Lu, Y. B. *et al.* Viscoelastic properties of individual glial cells and neurons in the CNS. *Proc. Natl Acad. Sci. USA* **103**, 17759–17764 (2006).
15. Mahaffy, R. E., Park, S., Gerde, E., Kas, J. & Shih, C. K. Quantitative analysis of the viscoelastic properties of thin regions of fibroblasts using atomic force microscopy. *Biophys J* **86**, 1777–1793 (2004).
16. Evans, K. E. & Alderson, A. Auxetic materials: Functional materials and structures from lateral thinking!. *Adv Mater* **12**, 617 (2000).
17. Trickey, W. R., Baaijens, F. P., Laursen, T. A., Alexopoulos, L. G. & Guilak, F. Determination of the Poisson's ratio of the cell: Recovery properties of chondrocytes after release from complete micropipette aspiration. *J. Biomech.* **39**, 78–87 (2006).
18. Moeendarbary, E. *et al.* The cytoplasm of living cells behaves as a poroelastic material. *Nature Mater.* **12**, 253–261 (2013).

19. Swift, J. *et al.* Nuclear lamin-A scales with tissue stiffness and enhances matrix-directed differentiation. *Science* **341,** 1240104 (2013).
20. Rowat, A. C. *et al.* Nuclear envelope composition determines the ability of neutrophil-type cells to passage through micron-scale constrictions. *J. Biol. Chem.* **288,** 8610–8618 (2013).
21. Booth-Gauthier, E. A., Alcoser, T. A., Yang, G. & Dahl, K. N. Force-induced changes in subnuclear movement and rheology. *Biophys. J.* **103,** 2423–2431 (2012).
22. Chowdhury, F. *et al.* Material properties of the cell dictate stress-induced spreading and differentiation in embryonic stem cells. *Nature Mater.* **9,** 82–88 (2010).
23. Dahl, K. N., Ribeiro, A. J. S. & Lammerding, J. Nuclear shape, mechanics, and mechanotransduction. *Circ. Res.* **102,** 1307–1318 (2008).
24. Mazumder, A., Roopa, T., Basu, A., Mahadevan, L. & Shivashankar, G. V. Dynamics of chromatin decondensation reveals the structural integrity of a mechanically prestressed nucleus. *Biophys. J.* **95,** 3028–3035 (2008).
25. Pajerowski, J. D., Dahl, K. N., Zhong, F. L., Sammak, P. J. & Discher, D. E. Physical plasticity of the nucleus in stem cell differentiation. *Proc. Natl Acad. Sci. USA* **104,** 15619–15624 (2007).
26. Meshorer, E. *et al.* Hyperdynamic plasticity of chromatin proteins in pluripotent embryonic stem cells. *Dev. Cell.* **10,** 105–116 (2006).
27. Chalut, K. J. *et al.* Chromatin decondensation and nuclear softening accompany Nanog downregulation in embryonic stem cells. *Biophys. J.* **103,** 2060–2070 (2012).
28. Masui, O. *et al.* Live-Cell Chromosome Dynamics and Outcome of X Chromosome Pairing Events during ES Cell Differentiation. *Cell.* **145,** 447–458 (2011).
29. Blumenfeld, R. & Edwards, S. F. Theory of strains in auxetic materials. *J. Supercond. Nov. Magn.* **25,** 565–571 (2012).
30. Nichols, J., Silva, J., Roode, M. & Smith, A. Suppression of Erk signalling promotes ground state pluripotency in the mouse embryo. *Development* **136,** 3215–3222 (2009).
31. Evans, M. J. & Kaufman, M. H. Establishment in culture of pluripotential cells from mouse embryos. *Nature* **292,** 154–156 (1981).
32. Plusa, B., Piliszek, A., Frankenberg, S., Artus, J. & Hadjantonakis, A. K. Distinct sequential cell behaviours direct primitive endoderm formation in the mouse blastocyst. *Development* **135,** 3081–3091 (2008).

Additional information

Supplementary information is available in the online version of the paper. Reprints and permissions information is available online at www.nature.com/reprints. Correspondence and requests for materials should be addressed to K.J.C.

Competing financial interests

The authors declare no competing financial interests.